Discrete ply model of circular pull-through test of fasteners in laminates

Louis Adam [a,b], Christophe Bouvet [b], Bruno Castanié [b,*], Alain Daidié [b], Elodie Bonhomme [a]

[a] Airbus, 316 Route de Bayonne, 31060 Toulouse Cedex 9, France
[b] Université de Toulouse, UPS, Mines d' Albi, ISAE, ICA (Institut Clément Ader), INSA, 135, Avenue de Rangueil, 31077 Toulouse Cedex, France

* Corresponding author. Tel.: +33 05 62 17 81 16; fax: +33 05 61 55 81 78.
E-mail address: bruno.castanie@insa-toulouse.fr (B. Castanié).

A B S T R A C T

In aeronautical structures, assemblies with thin laminates are becoming increasingly usual, especially for fuselage design. In these structures, out-of-plane loads can appear in bolted joints and can lead to progressive punching of the fastener's head in the laminate resulting, in some cases, in a failure mode called pull-through [1]. This complex phenomenon, which occurs in assemblies, was studied firstly by using a simplified "circular" pull-through test method. Qualitative micrographic examinations showed damage very similar to that observed in impacted specimens. The research presented here extends the Discrete Ply Model Method (DPM) developed by Bouvet et al. [2] to this case. The finite elements model is based on a particular mesh taking ply orientations into account. Cohesive elements are placed at the interfaces between solid elements to represent matrix cracks and delamination, thus allowing the natural coupling between these two damage modes to be represented. The model shows good correlation with test results, in terms of load/displacement curve, and correct prediction of the damage map until failure, including the splitting phenomenon.

Keywords:
Composite joints
Pull-through
Cohesive element
Experiment
FE modelling

1. Introduction

Bolted joints are extensively used in aeronautical structures. They have low sensitivity to environmental conditions and are easy to remove for inspection purposes. The behaviour of metallic bolted joints has been thoroughly studied in the past decades [3,4] for example. However, the increasing use of composite materials in aeronautical structures brings new design challenges. The high anisotropy of composite materials, especially for unidirectional laminates, and their brittle behaviour lead to complex failure modes [1,5–7]. Effects of localised stress concentrations and discontinuities induced by bolted connections must be evaluated under several loading cases, both in-plane and out-of-plane. The in-plane behaviour of composite joints has been studied widely but most authors have limited their work to single or double lap shear tests. The majority of studies focus on the modelling and experimental identification of damage in fastened joints or pinned holes [5–9], and on the influence of design: clearance, tightening effect or washer effects [10–16]. For thin laminates, the presence of secondary bending must be considered in order to accurately predict the failure of the assembly [17,18]. This secondary bending can introduce out-of-plane stresses in the laminate in the vicinity of the head (or the nut) of the fastener (Fig. 1). Out-of-plane stresses are also present in L-junctions (Fig. 2), which are particularly critical for thin laminates and new aircraft fuselages. Globally, less attention has been paid to out-of-plane failure modes.

One of the first studies was conducted by Freedman [19]. He analysed the out-of-plane loading caused by a hydraulic ram on a bolted assembly of a pressurised F-18 wing fuel tank. He noticed the significant sensitivity of composite laminates, compared to aluminium plates, towards this loading. This was confirmed by Waters and Williams [20] using a "push-through" test method, in which the fastener was pushed through a clamped laminate. Waters emphasised the major importance of interfaces on failure loads and described a complex failure pattern, ranging from intralaminar failures (i.e. matrix and fibre failure) to interlaminar failures (delamination). Kelly and Hallström [21] and Banbury and Kelly [22] also analysed the failure pattern of specimens subjected to out-of-plane loads. They introduced the analogy between this pattern and the "staircase" structure of impacted specimens. Top and bottom delaminations are linked by an inclined matrix crack, leading to the easily recognisable stacking of "top-hat" structures. This shows the interaction of matrix shear failure and delamination, as observed in impact loading [2]. Further investigations were performed to study the influence of joint parameters and predict the failure of the assembly. Banbury et al. [23] proposed a simplified axisymmetric model allowing the prediction of matrix failure as the primary mechanism, leading to delamination initiation and propagation. Elder et al. [24] introduced a simplified three-dimensional model using cohesive elements to represent delamination, which provided good prediction of the failure of quasi-isotropic laminates. Bunyawanichakul et al. [25] also studied the punching

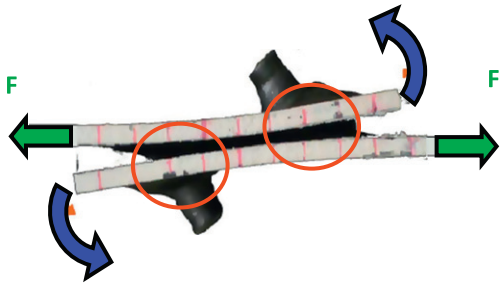

Fig. 1. Example of pull-through failure in single lap shear composite joints.

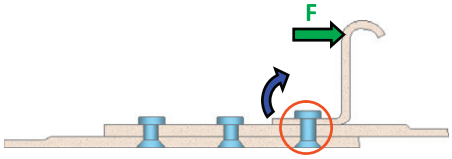

Fig. 2. Pull-through in thin L-Joints.

of a laminate as the last failure mode of pull-out of inserts in sandwich structures. In this case, transverse shear was practically the only phenomenon that had to be taken into account and a two-step damage law was proposed. The first step corresponded to matrix shear cracking and the final failure was due to transverse shear fibre failure. More recently, Catalanotti et al. [26] proposed an experimental and numerical study of pull-through of glass-fibre-reinforced plastic laminate joints used in railway transportation. The major focus was on the sub-critical initial failure, identified as onset of delamination. This failure was accurately predicted using linear elastic elements and cohesive elements.

Most studies are based on circular boundary conditions as described in ASTM D7332, method B [27]. The main difference lies in the clamped or simply supported boundary condition. The influence of the support diameter (defined as the *clearance hole diameter* in ASTM D7332) was found to be insignificant for the failure load in the range considered [20].

The aim of this paper is to propose an experimental and numerical study of the pull-through of fasteners in carbon/epoxy laminates so as to better understand and predict the failure mechanisms. Tests using actual joint geometries, such as L-junctions or single lap shear, are complex and difficult to model. A simplified geometry inspired by ASTM D7332 (method B), and called "circular pull-through", is chosen here, with several fastener sizes and support diameters. Based on the experimental analogy with impact-induced damage, a finite element model inspired by the low-energy, low-velocity impact model of Bouvet et al. [2] is then proposed to predict the damage scenario of laminates under out-of-plane loading.

2. Experimental study

2.1. Description of pull-through tests and specimens

The pull-through test rig is presented in Fig. 3. This test method is close to one proposed by Military Handbook 17A [1] or ASTM D7332 [26]. The carbon/epoxy laminate, in which a threaded

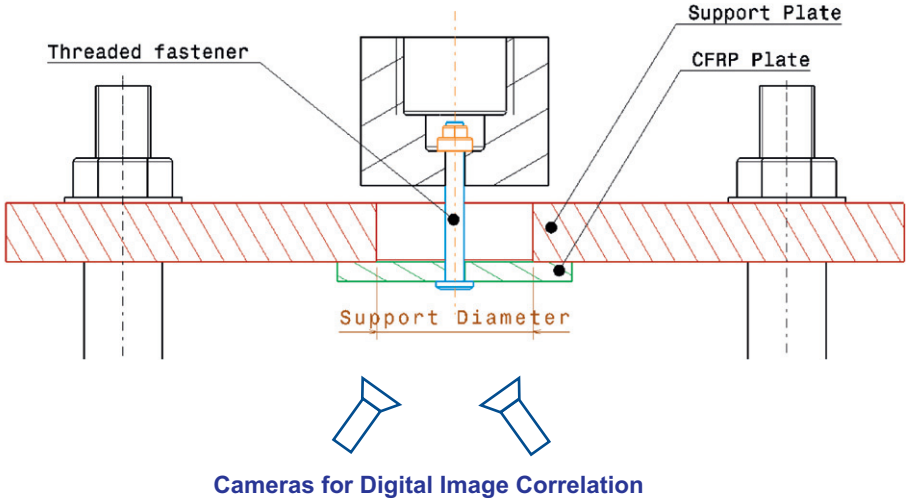

Fig. 3. Pull-through test principle and photo.

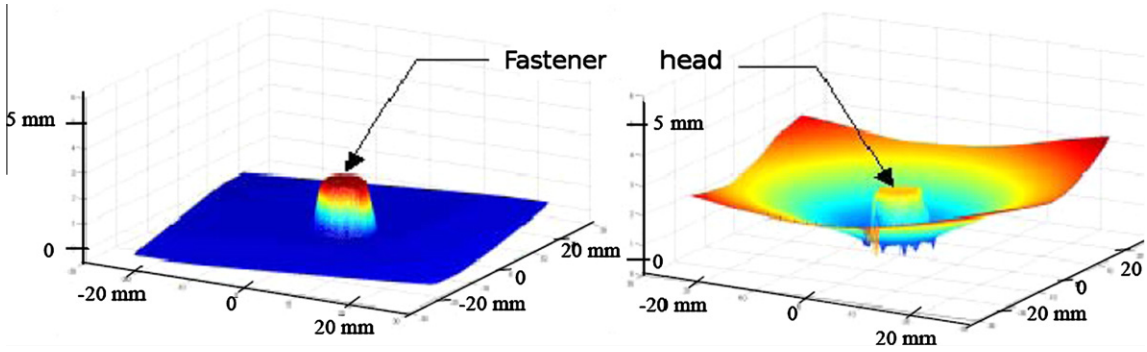

Fig. 4. Digital Image Correlation results (left: beginning of test, right: during test).

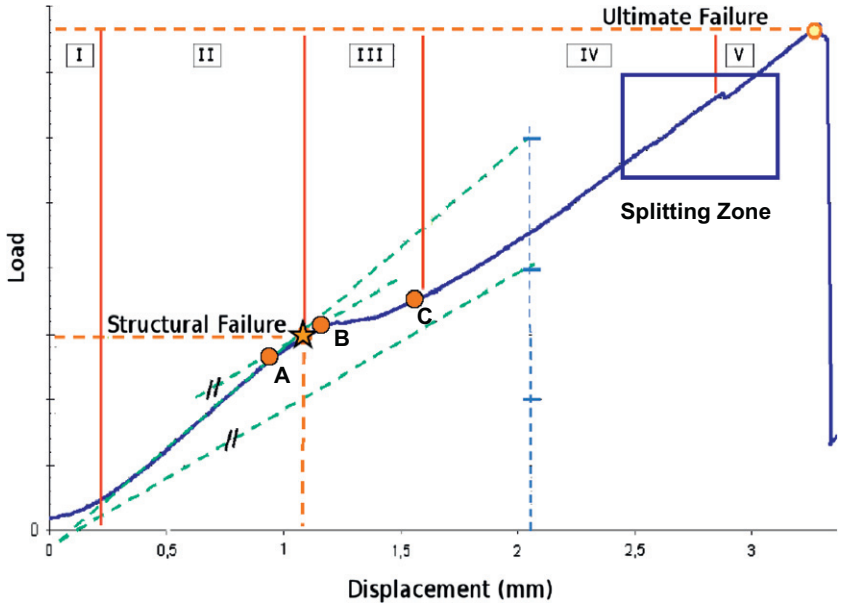

Fig. 5. Typical load/displacement curve of a circular pull-through test.

fastener is installed, is simply supported on a diameter of a metallic support plate. The fastener is held in the tensile machine by a dedicated fixture. The crosshead displacement, at 0.5 mm/min, pulls the screw through the specimen, creating in-plane and out-of-plane stresses in the specimen. Two CCD cameras are focused on the lower face of the laminate, allowing its field of displacement to be measured by Digital Image Correlation (DIC). Data are processed by the commercial software Vic3D and then post-treated in Matlab (Fig. 4). They are then merged with those from the load cell in order to establish load/displacement curves used for comparison with numerical simulations. For an accurate comparison with numerical results, the actual value of the displacement is the difference between the laminate displacement at the support diameter and the displacement of the head. Due to the high stiffness of the laminate, displacements are very small (less than 1 mm for the smallest support diameter), leading to potential accuracy issues on displacement measurement.

Previous studies [20,21] showed no influence of the support diameter for ratios of support diameter to fastener head diameter of 5–20 Nevertheless, it seemed important to study the influence of the support diameter for lower values, close to pure punching. Due to the variation of out-of-plane shear stresses with the head diameter, this parameter has a significant influence [26]. On this basis, the following parameters were chosen:

- Thickness: 2 mm (stacking sequence [+45; −45; 0; 90; +45; −45]s).
- Fastener shank diameters: 4.8 and 6.35 mm.
- Support diameters: 15, 20 and 40 mm.
- Material: carbon/epoxy.

The specimens were square plates, with edge lengths of 35, 40 and 60 mm for the three support diameters. For each configuration, five specimens were used, leading to a total of 30 tests.

2.2. Experimental results

The five tests performed for each configuration showed low scatter. A typical load/displacement curve is shown on Fig. 5. It can be decomposed into five main steps:

- Step I: Contact establishment.
- Step II: Linear elastic behaviour.
- Step III: Stiffness decrease, with first audible cracks: structural failure.
- Step IV: Stiffness increase due to membrane effect, followed by apparently constant stiffness.
- Step V: Ultimate failure of the laminate, often preceded by minor load drops.

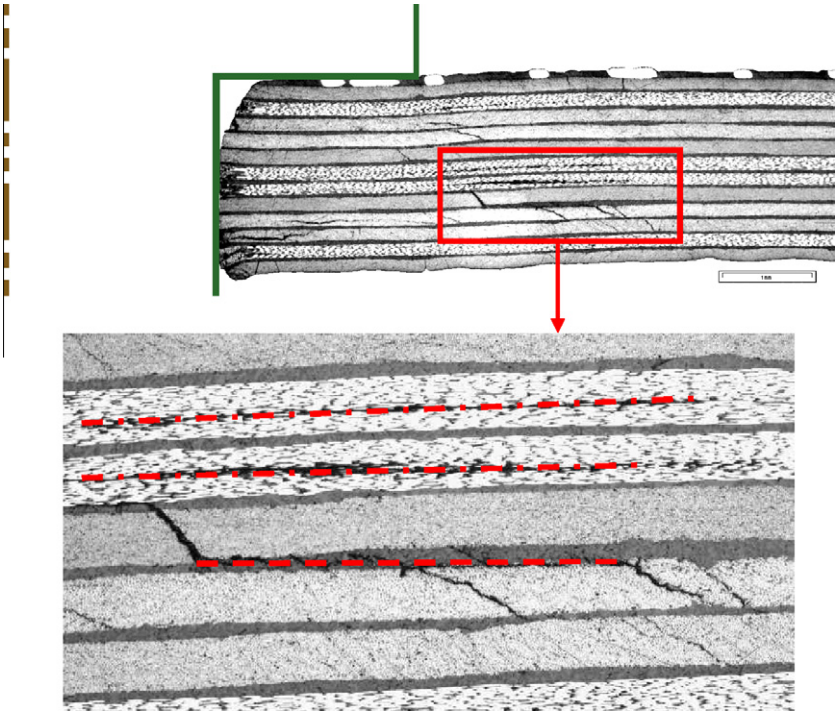

Fig. 6. Post-mortem analysis of the damaged region.

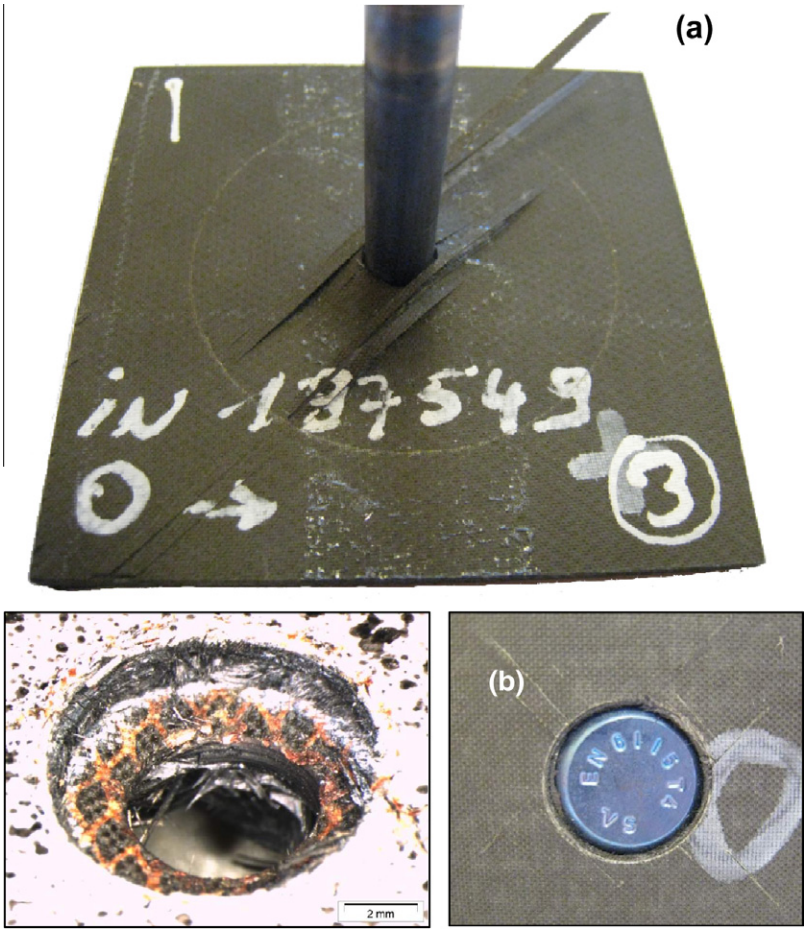

Fig. 7. Post-mortem failure pattern of a specimen showing splitting and punching.

Table 1
Normalized values of failure loads.

Ref.	Shank diameter (mm)	Head diameter (mm)	Support diameter (mm)	Structural failure	Ultimate failure	ρ
A15	4.80	9.3	15	0.33	0.80	0.41
A20			20	0.38	0.68	0.55
A40			40	0.38	0.52	0.72
B15	6.35	10.9	15	0.39	1.00	0.39
B20			20	0.41	0.75	0.55
B40			40	0.40	0.57	0.72

The definition of the structural failure was based on the concept of "no crack growth". This meant that, under the associated structural failure load, no crack propagated inside the structure. The decrease in stiffness and audible noise at the beginning of step III were an indication of delamination onset. Based on these observations and in accordance with ASTM 7332, the structural failure load was given by a slope change (greater than 10%) or minor load drops (less than 10%). As expected and as found in the literature [26], the structural failure load was much lower than the ultimate failure load.

Post-mortem micrographic examination confirmed the observations made by Banbury et al. [22]. We observed a "staircase" damage pattern, composed of transverse shear matrix failures, leading to delaminations (Fig. 6). Less usual intraply delaminations, specific to laminates presenting high interface toughness [20], were observed. The precursor role of matrix cracks on delamination onset was observed as in impacted specimens, showing the importance of taking the interaction between intralaminar and interlaminar damage into account. Splitting occurred in step IV on the head and support sides (see Fig. 5: Splitting area). Higher transverse tensile stresses due to the bending of the specimen tended to facilitate the apparition of splitting located in the vicinity of the head on the support side (Fig. 7a). Finally, the ultimate failure occurred by punching of the laminate skin by the screw head (Fig. 7b).

Average values of structural and failure loads are presented in Table 1. ρ is introduced as the ratio of structural to ultimate failure loads. Increasing the support diameter decreases the ultimate load, due to additional bending stresses, but does not affect the structural failure. As noted by Catalanotti et al. [26], increasing the bolt diameter increases both the structural and ultimate failure load. To be able to study the failure scenario in more detail, some tests were interrupted at 90% (Specimen A), 100% (first audible crack, Specimen B) and 120% (Specimen C) of the structural failure load (see points on Fig. 5) and the micrographs are shown in Fig. 8. The first one shows no visible damage. Specimen B exhibits a first staircase pattern and the last specimen shows propagation of delamination with intra-ply damage. This confirms the failure scenario, which is close to the scenario observed in low-velocity, low-energy impact on laminates.

3. Finite element modelling

As for impact, it is essential to take the interaction between intralaminar and interlaminar damage into account for correct prediction of pull-through failure. Actually, one of the most efficient modelling strategies for this subject seems to be the use of cohesive elements associated with discrete ply modelling [2,28]. Thus, since the modelling strategy proposed by Bouvet et al. [2] has provided good results for impact, this approach was extended here to the analysis of circular pull-through. The main key points of this approach are presented below, with slight differences relative to the initial version published in [2].

As in the original model, in order to represent the "staircase" damage pattern, the mesh follows the orientations of the plies (Fig. 9). Cohesive elements called "delamination elements" represent interply interfaces. Plies are divided into strips, which are linked together by cohesive elements called "matrix shear elements" (Figs. 9 and 10). Four nodes correspond to each geometric point. To create a hole, elements in the hole area are deleted. This constraint leads to a discontinuous mesh around the hole (Fig. 10). Experimental study has shown that damage initiates far from the

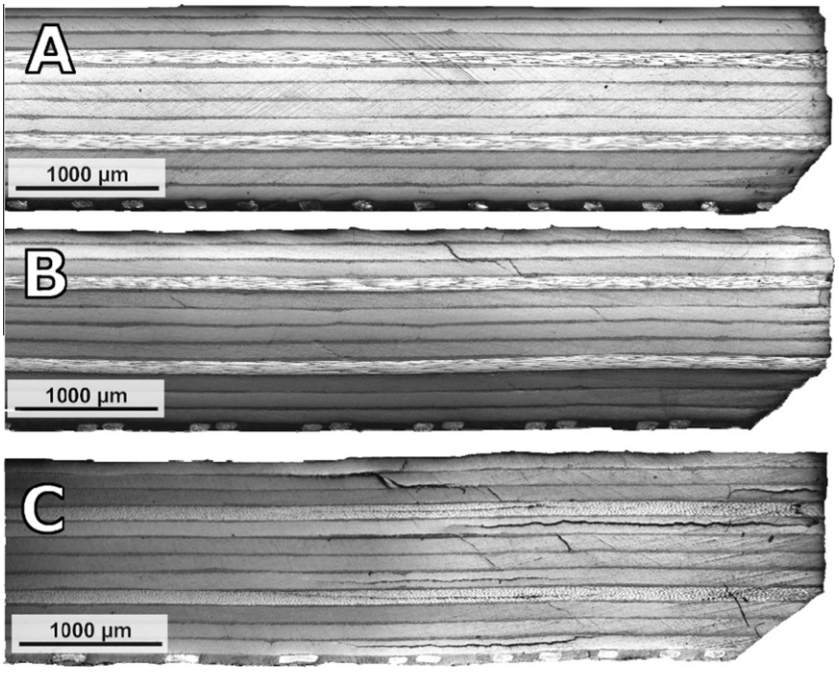

Fig. 8. Micrographs after test stopped at 90% (Specimen A and point A Fig. 5), 100% (Specimen B) and 110% (Specimen C and point C Fig. 5) of the structural failure load.

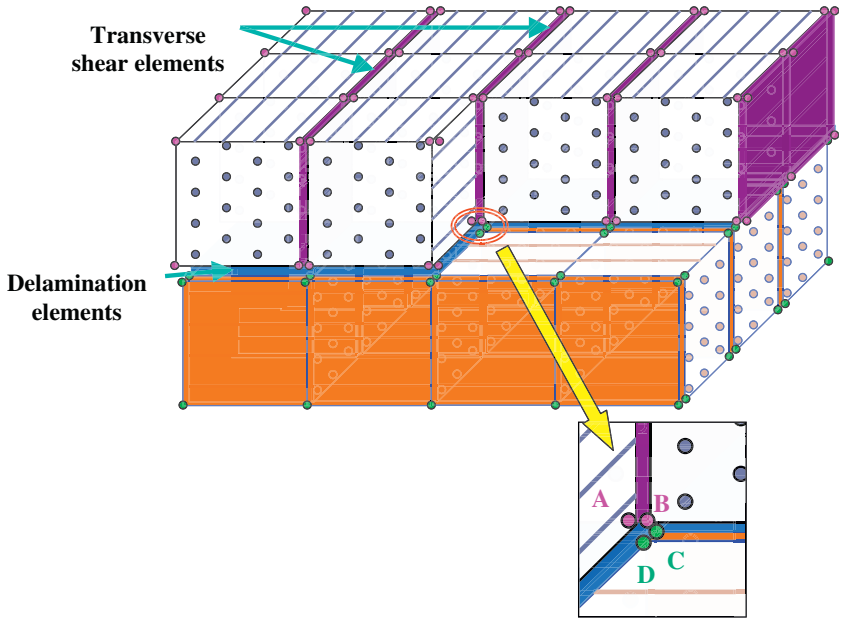

Fig. 9. Meshing principle.

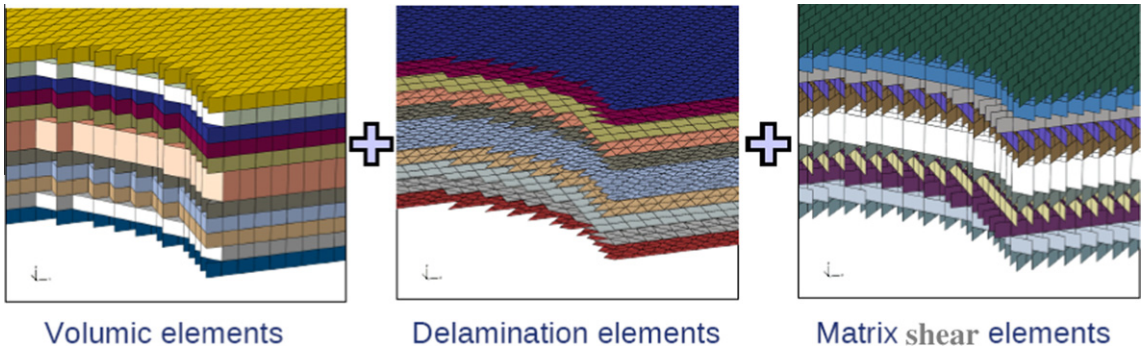

Fig. 10. Overview of mesh near the hole.

edge of the hole. Simulations with non-damageable cohesive elements in the vicinity of the hole have shown very similar results compared to all-damageable models. Mesh sizes of 0.2 and 0.5 mm have led to the same structural failure prediction. Discontinuities created by the hole and its tessellation do not seem to influence the simulation results with current mesh sizes. This is consistent with experimental observations, showing little or no damage onset around the hole (Figs. 6 and 8).

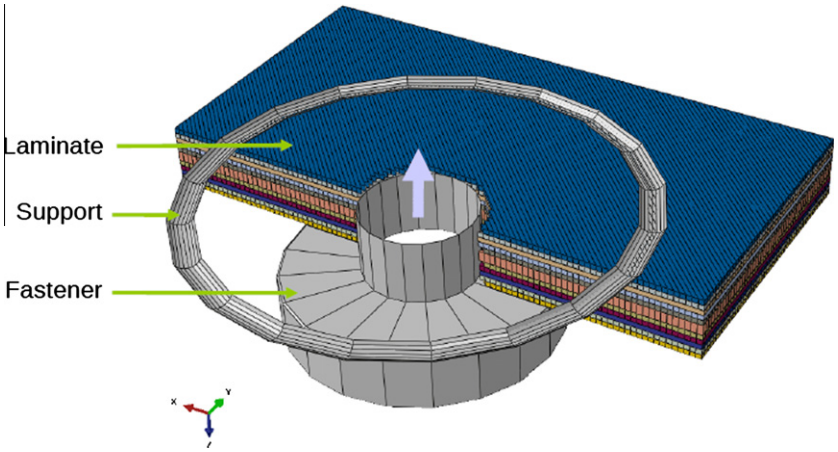

Fig. 11. Overview of model.

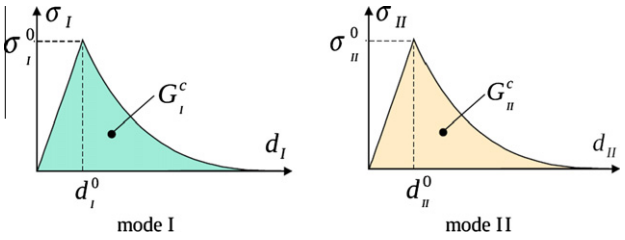

Fig. 12. Cohesive law for delamination elements.

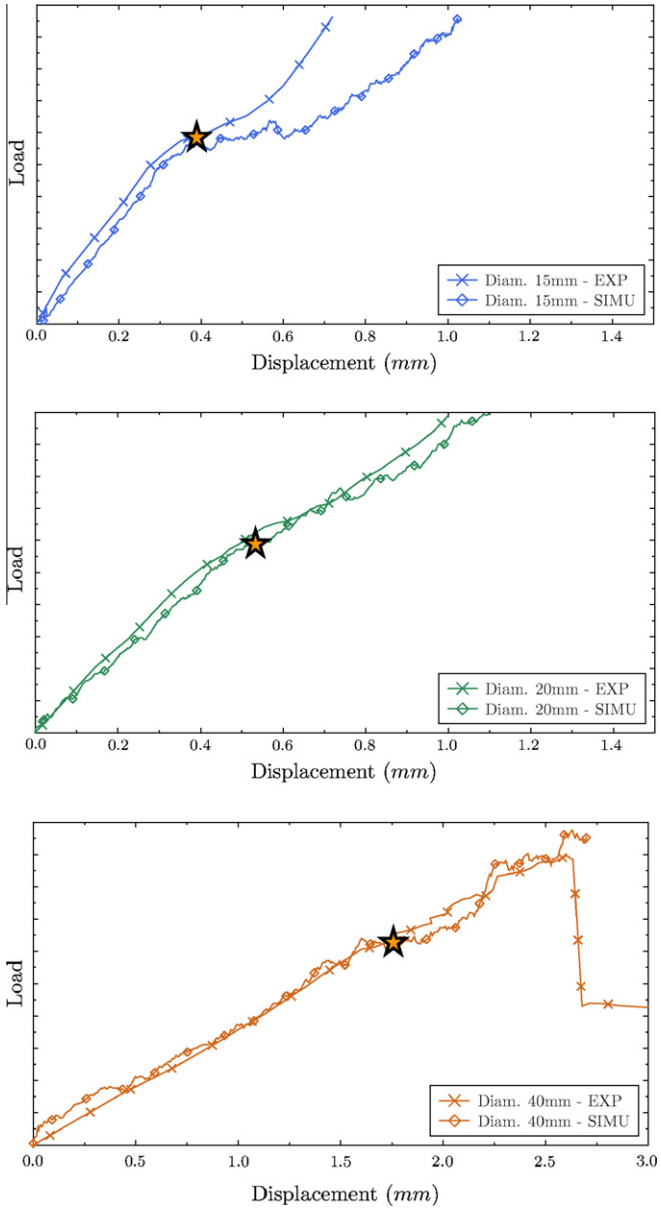

Fig. 13. Model/experiment comparison in terms of load/displacement curves (the stars represent "structural failure").

Ply elements are C3D8, with non-reduced integration to ensure correct bending behaviour with only one element in the thickness of each ply. The explicit resolution method was chosen to ensure the convergence of the simulation despite high numerical instability. It is also more efficient on High-Performance Computation centres.

To decrease the computation time, only half of the laminate is modelled (Fig. 11). An axial anti-symmetry is then introduced to model the other half. Compliances of the fastener head and of the support plate are neglected, allowing the use of a rigid body to model these parts. The load is then introduced as a displacement of the fastener's head. The Abaqus software allows the use of specific behaviour laws thanks to user subroutines, especially the Vectorized User MATerial for Abaqus/Explicit. This subroutine manages both the linear and the damaged behaviour of all the elements of the model. Tensile and compressive states in the longitudinal direction are taken into account for the elastic behaviour of the ply elements.

Transverse shear failure is evaluated through a quadratic criterion on the ply volume elements (Eq. (1)). Each cohesive element of matrix cracking interrogates the 2 ply volume elements close to it, and is considered as broken when the criterion is reached for at least one of them:

$$\left(\frac{\max(\sigma_{tt},0)}{\sigma^r}\right)^2+\frac{\sigma_{lt}^2+\sigma_{tz}^2}{(\tau^r)^2}<1 \tag{1}$$

where σ^r is the transverse tensile strength and τ^r the shear strength.The behaviour of matrix shear cohesive elements is taken into account by a single stiffness K_f (Eq. (2)). It is chosen sufficiently large at the initial state to represent the intact behaviour. When the element is broken, this stiffness, K_f, is reduced to zero. Once again, the failure of these elements is managed by the stresses of their neighbouring ply volume elements, and not by their own stresses σ_{33}, τ_{13} and τ_{23}:

$$\begin{pmatrix}\sigma_{33}\\ \tau_{13}\\ \tau_{23}\end{pmatrix}=K_f\begin{pmatrix}d_{33}\\ d_{13}\\ d_{23}\end{pmatrix} \tag{2}$$

where σ_{33} (d_{33}) is the normal stress (displacement), τ_{13} (d_{13}) and τ_{23} (d_{23}) the shear stresses (displacements).

The behaviour of delamination cohesive elements (see Fig. 12) follows an approach in energy release rate. In this case, two stiffnesses are introduced: K_I in normal stress, and K_{II} in shear stress (Eq. (3)):

$$\begin{pmatrix}\sigma_{33}\\ \tau_{13}\\ \tau_{23}\end{pmatrix}=\begin{pmatrix}K_I\\ K_{II}\\ K_{II}\end{pmatrix}\cdot\begin{pmatrix}d_{33}\\ d_{13}\\ d_{23}\end{pmatrix} \tag{3}$$

The mixed-mode relation is given by a simple linear criterion (Eq. (4)). Because of the lack of data for mode *III*, modes *II* and *III* are assumed equivalent.

$$\frac{G_I}{G_I^c}+\frac{G_{II}}{G_{II}^c}+\frac{G_{III}}{G_{III}^c}=1 \tag{4}$$

The displacements and stresses are then given as follows:

- in mode *I*: $d_I = d_{33}$ and $\sigma_I = \sigma_{33}$,
- in mode *II*: $d_{II}=\sqrt{d_{13}^2+d_{23}^2}$ and $\sigma_{II}=\sqrt{\sigma_{13}^2+\sigma_{23}^2}$.

where d_I (d_{II}) is the displacement in mode *I* (*II*), and σ_I (σ_{II}) the stress in mode *I* (*II*). The initiation criterion is based on maximum displacement, for each mode. Equivalent and critical displacement are given by:

- Equivalent displacement:

$$\text{in tension}(d_I>0): \quad d_{eq}=\sqrt{(d_I)^2+\left(\frac{d_I^0}{d_{II}^0}d_{II}\right)^2}$$

$$\text{in compression}(d_I<0): \quad d_{eq}=d_{II}+\lambda d_I$$

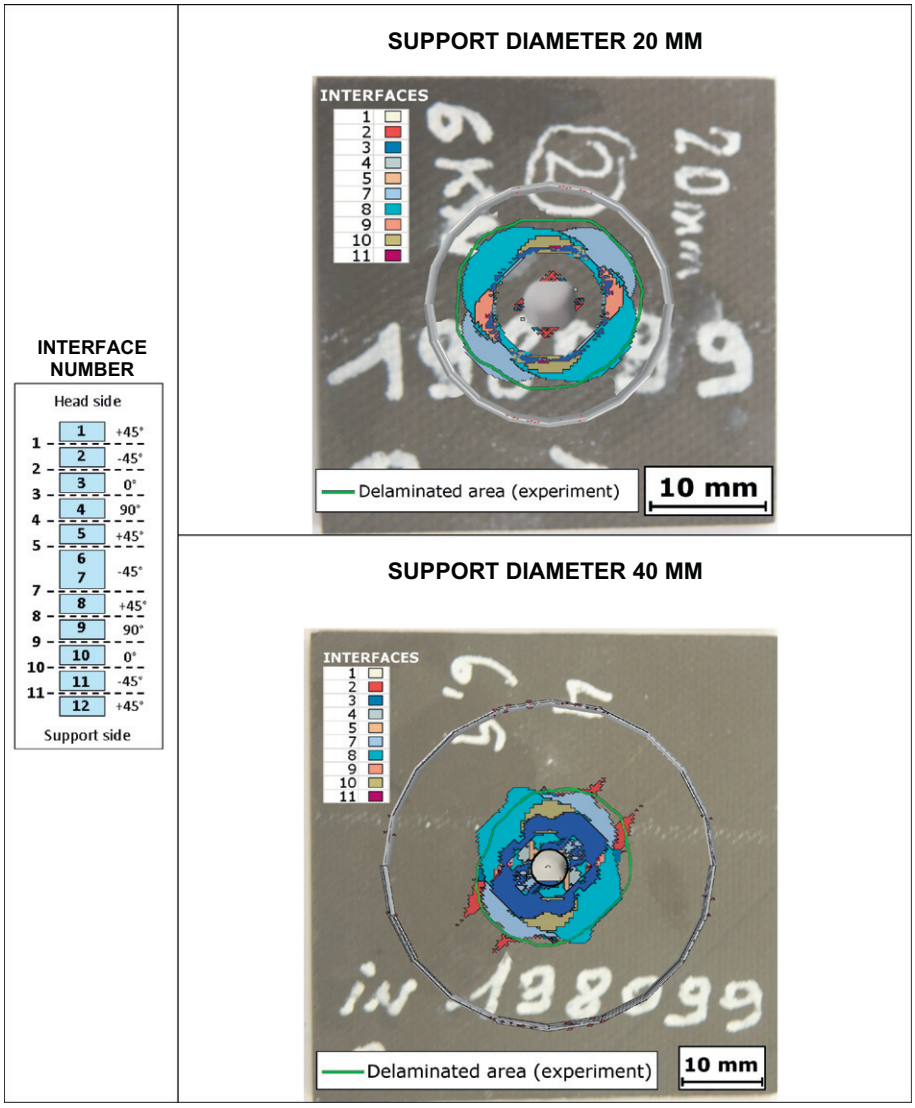

Fig. 14. Comparison of simulated and measured delaminated areas at structural failure.

– Critical displacement:

in mode I : $d_I^0 = \dfrac{\sigma_I^0}{K_I^0}$

in modeII : $d_{II}^0 = \dfrac{\sigma_{II}^0}{K_{II}^0}$

where $K_I^0 (K_{II}^0)$ is the initial stiffness in mode I (II) and σ_I^0 (σ_{II}^0) the limit stress in mode I (II) which is assumed equal to the transverse tensile (shear) strength σ^r (τ^r). The λ parameter is defined to take account of the positive effect of compression on delamination propagation in mode II, as observed by Hou et al. [29]. Associated stresses in mode I and II are given by Eq. (5) and represented in Fig. 11:

$$\sigma_I = \sigma_I^0 \exp(-\beta(d_{eq} - d_{Ic}))\frac{d_I}{d_{eq}}$$
$$\sigma_{II} = \sigma_{II}^0 \exp(-\beta(d_{eq} - d_{Ic}))\frac{d_{II}}{d_{eq}}\frac{d_I^0}{d_{II}^0} \quad (5)$$

To dissipate G_I^c in mode I, we impose $\beta = \dfrac{1}{\dfrac{G_I^c}{\sigma_I^0} - \dfrac{d_I^0}{2}}$.

The initial stiffness in mode II is then given by $K_{II}^0 = \dfrac{(\sigma_{II}^0)^2}{G_{II}^c}\left(\dfrac{1}{2} + \dfrac{1}{\beta \cdot d_I^0}\right)$ to dissipate G_{II}^c in mode II with the same coefficient β as in mode I.

The material parameters to be defined are then σ_I^0 (equal to σ^r), σ_{II}^0 (equal to τ^r), G_I^c, and $G_{II}^c \cdot K_I^0$, ideally infinite, is chosen by numerical considerations.

4. Experimental and numerical comparison

Numerical results were compared with experimental ones in terms of load/displacement curves and in terms of failure pattern and scenario. The model was validated for a fastener diameter of 4.8 mm. Good correlation was found for the initial stiffness and for the structural failure, for all support diameters (Fig. 13). Globally, the model tended to underestimate the structural failure load by about 10%. For the smallest diameter of support, after the structural failure, the correlation was less relevant but the model was conservative. The discrepancy was probably due to a bad estimation of the damaged transverse shear stiffness.

Delamination was not observed either in the model or in experiments (Fig. 8a) before structural failure. The delaminated areas

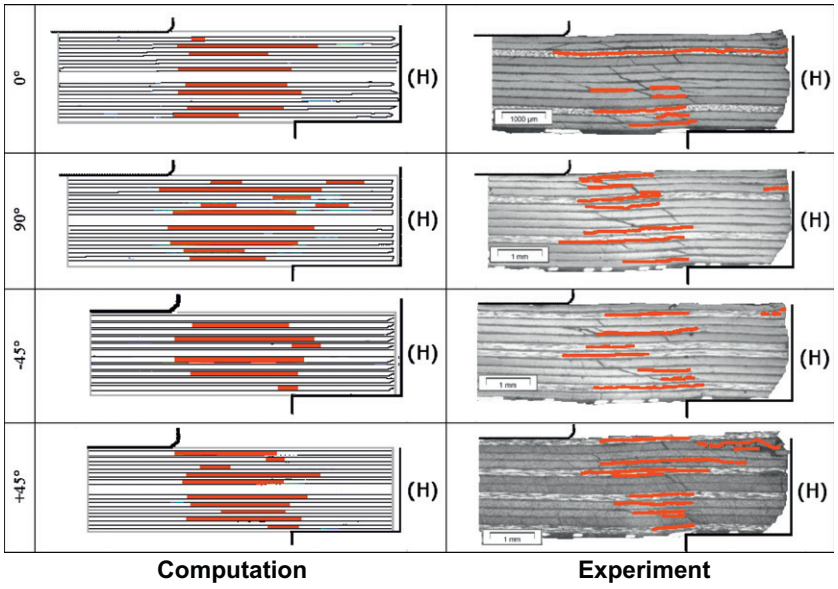

Fig. 15. Comparison of delaminated interfaces (diameter 15 mm, at structural failure).

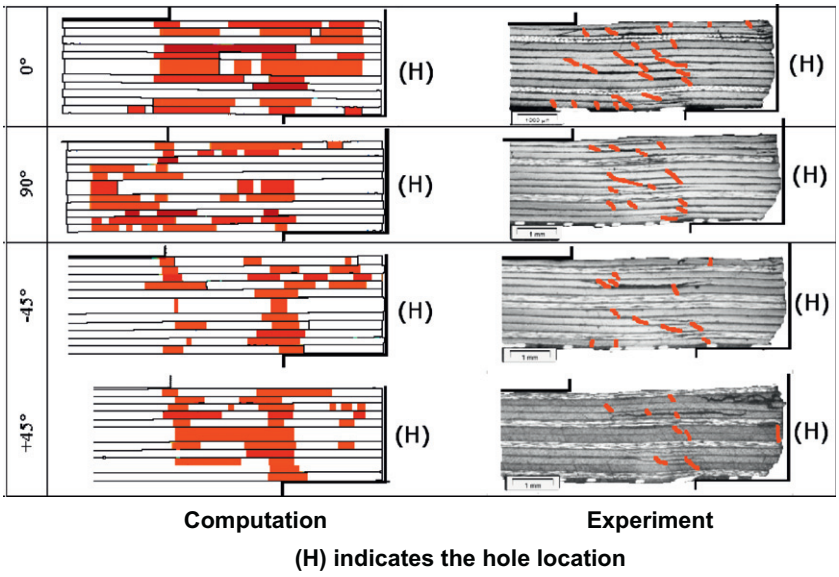

Fig. 16. Comparison of matrix shear failure (diameter 15 mm, at structural failure).

just after structural failure (point B) are compared in Fig. 14. Due to the small size of the specimens, C-Scan ultrasonic inspections were not possible near the hole, thus only the outer border is drawn and the comparison of exact delaminated interfaces was not performed. Globally, the same patterns were observed between experiment and prediction. To confirm this point, micrographic cuts were also performed for 0°, +45°, 90° and −45° planes for a diameter of 15 mm. Again, the global comparison was good in terms of matrix failure and delamination patterns (Figs. 15 and 16). Intraply delaminations were observed in experiments but could not be simulated. For convenience of comparison, these delaminations were considered as happening in the ply immediately above or below. Globally, the same damage localisation was found in simulation and experiments, especially for the non-damaged cylinder above the fastener head. However, matrix shear failure seemed to be more present in simulation (which can explain why the shear stiff-

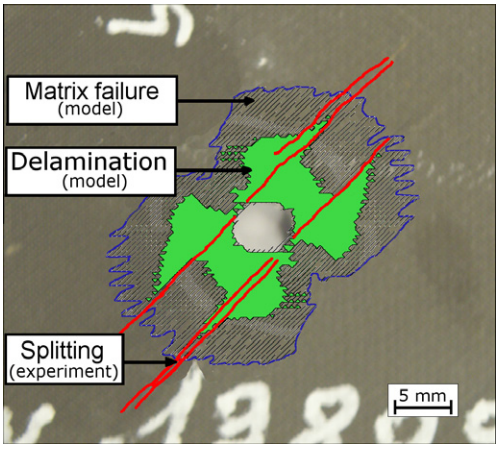

Fig. 17. Simulated delamination of the first interface on support side (N°11, see Fig. 14) and experimental splitting.

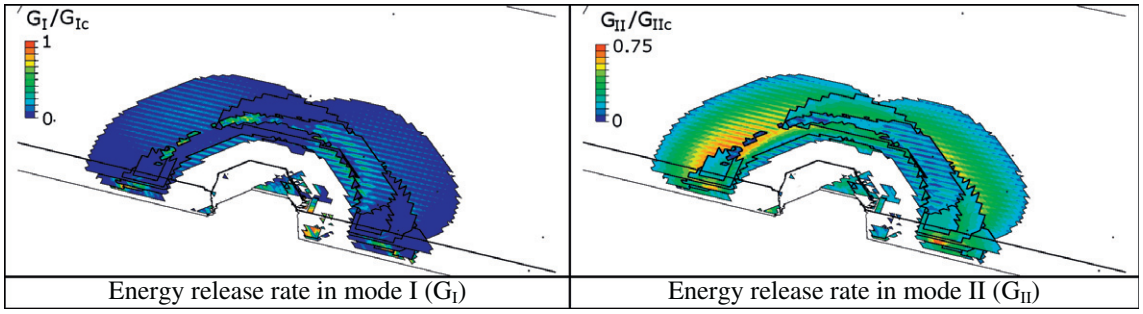

Fig. 18. Energy release rates in modes *I* and *II* of delaminated interfaces after the structural failure.

ness after structural failure is lower in simulation, (Fig. 13)). Also, some delamination in tests seemed to extend to the hole.

An interesting pattern was found for the delamination of the first ply interface on the support side (Fig. 17) in the splitting area (Fig. 5). This pattern presented four branches which could be superimposed on the split strips. Therefore, it seems that the phenomenon of splitting is related to this pattern. It was naturally captured by the model, probably because of the natural intra-interlaminar coupling. Nevertheless, the simulated splitting was less than that found experimentally, probably because the damage around the hole was not taken into account correctly by the modelling strategy. After splitting, close to ultimate failure, extensive delamination was observed, bounded by the support diameter. To understand this delamination better, energy release rates in modes *I* and *II* were compared and showed a preponderant propagation of delaminations in mode *II* (Fig. 18) after the structural failure, which is also the case for impact. Finally, unlike the model proposed by Bunyawanichakul et al. [25], this model is not able to take account of the punch failure (Fig. 7b), which is the ultimate failure mode.

5. Conclusions

This study was dedicated to failure analysis and modelling of a circular pull-through test on a thin carbon/epoxy laminate. Based on the resemblance in terms of failure scenario with the low-energy impact damage, discrete cohesive finite element modelling was developed and adapted to this issue. The structural failure load was taken at the onset of delamination. It was concomitant with the first audible noises detected. From an experimental point of view, no influence of the support diameter on the structural failure was observed, which seems to confirm the major influence of out-of-plane shear stresses and the coupling between transverse shear failure and delamination. The model is based on a discrete representation of the plies, using cohesive elements both for delamination and for matrix transverse shear failure. It allows precise prediction of the structural failure for the support diameters considered. The failure scenario is well reproduced, and the delaminated area correlated. The location of the damage corresponds to the experimental observations. The model is also able to predict splitting for the ultimate loads. The ultimate load is not well predicted at the moment, and would require additional investigation. Further experiments are also needed to accurately measure energy restitution rates in mode *I* and mode *II* for various adjacent orientations.

Acknowledgements

The research leading to these results received funding from the European Community's Seventh Framework Programme FP7/2007-2013 under grant agreement 213371 (MAAXIMUS – www.maaximus.eu).

References

[1] US Mil-Hbk 17A, Chapter 7: Structural element characterization.
[2] Bouvet C, Castanié B, Bizeul M, Barrau J-J. Low velocity impact modelling in laminate composite panels with discrete interface elements. Int J Solids Struct 2009;46:2809–21.
[3] Alkatan F, Stephan P, Daidie A, Guillot J. Equivalent axial stiffness of various components in bolted joints subjected to axial loading. Finite Elem Anal Des 2007;43(8):589–98.
[4] Fares Y, Chaussumier M, Daidie A, Guillot J. Determining the life cycle of bolts using a local approach and the Dang Van criterion. Fatigue Fract Eng Mater Struct 2006;29(8):588–96.
[5] Hung C-L, Chang F-K. Strength envelope of bolted composite joints under bypass loads. J Compos Mater 1996;30:1402–35.
[6] Valenza A, Fiore V, Borsellino C, Calabrese L, DiBella G. Failure map of composite laminate mechanical joint. J Compos Mater 2007;41:951–64.
[7] Castanié B, Creze S, Barrau JJ, Lachaud F, Risse L. Experimental analysis of failure in filled hole compression tests. Compos Struct 2010;92(5):1192–9.
[8] Persson E, Madenci E, Eriksson I. Delamination initiation of laminates with pin loaded holes. Theor Appl Fract Mec 1998;30:87–101.
[9] Ireman T, Ranvik et T, Erikksson I. On damage development in mechanically fastened composite laminates. Compos Struct 2000;49(2):151–71.
[10] McCarthy MA, Lawlor VP, Stanley WF, McCarthy CT. Bolt-hole clearance effects and strength criteria in single-bolt, single-lap, composite bolted joints. Compos Sci Technol 2002;62:1415–31.
[11] Naik RA, Crews JH. Stress analysis method for clearance fit-bolt under bearings load. AIAA J 1985;24:1348–53.
[12] Tong L. Bearing failure of composite bolted joints with non-uniform bolt-to-washer clearance. Compos Part A: Appl Sci Manuf 2000;31:609–15.
[13] Park H-J. Effects of stacking sequence and clamping force on the bearing strengths of mechanically fastened joints in composite laminates. Compos Struct 2001;53:213–21.
[14] Park H-J. Bearing failure analysis of mechanically fastened joints in composite laminates. Compos Struct 2001;53:199–211.
[15] Wang H-S, Hung C-L, Chang F-K. Bearing failure of bolted composite joints. Part I: Experimental characterization. J Compos Mater 1996;30(12):1284–313.
[16] Hung C-L, Chang F-K. Bearing failure of bolted composite joints. Part II: Model and verification. J Compos Mater 1996;30(12):1359–400.
[17] Ekh J, Schön J, Melin L. Secondary bending in multi fastener, composite-to-aluminium single shear lap joints. Compos Part B 2005;36(3):195–208.
[18] Ekh J, Schön J. Effect of secondary bending on strength prediction of composite, single shear lap joints. Compos Sci Technol 2005;65(6):953–65.
[19] Freedman RN. A study of pull-through failures of mechanically fastened joints, Master Thesis, Naval Postgraduate School, Monterey, California; 1977.
[20] Waters WA, Williams JG. Failure mechanisms of laminates transversely loaded by bolt push through. NASA Technical Memorandum TM 87603; 1985.
[21] Kelly G, Hallström S. Strength and failure mechanisms of composite laminates subject to localised transverse loading. Compos Struct 2005;69:301–14.
[22] Banbury A, Kelly D. A study of fastener pull-through failure of composite laminates. Part 1: Experimental. Compos Struct 1999;45(4):241–54.
[23] Banbury A, Kelly D, Jain L. A study of fastener pull-through failure of composite laminates. Part 2: Failure prediction. Compos Struct 1999;45(4):255–70.
[24] Elder D, Verdaasdonk A, Thomson R. Fastener pullthrough in a carbon fibre epoxy composite joint. Compos Struct 2008;86(1-3):291–8.
[25] Bunyawanichakul P, Castanié B, Barrau JJ. Nonlinear finite element analysis of inserts in sandwich structures. Compos Part B 2008;39:1077–92.
[26] Catalanotti G, Camanho PP, Ghys P, Marques AT. Experimental and numerical study of fastener pull-through in GFRP laminates. Compos Struct 2011. http://dx.doi.org/10.1016/j.compstruct.2011.06.02.
[27] ASTM D7332 / D7332M – 09 Standard test method for measuring the fastener pull-through resistance of a fiber-reinforced polymer matrix composite.
[28] Wisnom MR. Modelling discrete failures in composites with interface elements. Compos Part A 2010;11(7):795–805.
[29] Hou JP, Petrinic N, Ruiz C. A delamination criterion for laminated composites under low-velocity impact. Compos Sci Technol 2001;61:2069–74.